



Effect of Cerium on the Electrical Properties of a Cobalt Conversion Coating for Solid Oxide Fuel Cell Interconnects – A Study Using Impedance Spectroscopy



Jan Gustav Grolig*, Jan Froitzheim, Jan-Erik Svensson

Environmental Inorganic Chemistry, Chalmers University of Technology, Kemivägen 10, 41296 Gothenburg, Sweden

ARTICLE INFO

Article history:

Received 2 July 2015

Received in revised form 19 October 2015

Accepted 20 October 2015

Available online 26 October 2015

ABSTRACT

Coatings of metallic cobalt, which convert into a cobalt manganese spinel oxide are known to improve the properties of interconnects for solid oxide fuel cells (SOFCs). The addition of cerium to the cobalt coating further improves the corrosion properties of the material. For this study traditional four-point DC measurements at high temperatures were combined with impedance spectroscopy at low temperatures in order to investigate the effect of cerium on the electrical properties of a cobalt conversion coating. It was found that combination-coatings of cerium and cobalt exhibit superior electrical properties compared to pure cobalt coatings. Cerium slows down the growth of chromia and prevents the outward diffusion of iron into the cobalt spinel layer. Both effects are beneficial for the electrical properties of the interconnect. Impedance spectroscopy measurements revealed that even after more than 3000 h of exposure the outer cobalt manganese spinel layer still has a higher electrical conductivity when cerium was present.

© 2015 The Authors. Published by Elsevier Ltd. This is an open access article under the CC BY-NC-ND license (<http://creativecommons.org/licenses/by-nc-nd/4.0/>).

1. Introduction

Solid oxide fuel cells (SOFCs) are recognized as an interesting alternative technology for electricity and heat production. Several planar fuel cell elements are usually connected in series to reach sufficient power densities. This is achieved by the utilization of so-called interconnector plates or interconnects. Recent developments, such as improved cathode performance and thinner electrolytes, have led to lower operational temperatures and thus have allowed the use of interconnects fabricated of metallic materials. Extensive research has led to the development and investigation of several suitable alloys for use as interconnects. Examples of these are Crofer 22 APU and Crofer 22H from VDM ThyssenKrupp, Sanergy HT from Sandvik Materials Technology or ZMG 232 from Hitachi Materials [1–3]. Other non-specific SOFC application developments such as AISI 430 or 441 have also been reported [4–6]. The degradation of the interconnect is a major limiting factor for the life-time of SOFC stacks [7]. Three major degradation mechanisms can be identified that degrade interconnect performance; the evaporation of chromium, the oxidation of the metal, and an increase in electrical resistance due to the

oxidation process. Metallic cobalt conversion coatings have shown great potential in overcoming the issues of chromium evaporation and increasing electrical resistance [8–10]. The combination of a cobalt conversion coating with cerium has previously been shown to improve the corrosion resistance of interconnect materials [4,9,11]. Previous studies on these coatings have shown that the metallic cobalt coating is oxidized to Co_3O_4 in the very first moments of exposure [9,10]. With time, manganese, which is contained in the steel, diffuses outwards to the Co_3O_4 spinel converted cobalt coating. Canovic et al. have shown a significantly higher amount of iron in the outer spinel layer when only cobalt is used, in contrast to an almost iron-free outer spinel when a cobalt coating is applied onto a 10 nm thick cerium layer [9]. The cobalt manganese spinel acts as a cap layer and decreases the evaporation of chromium and can, in some cases, even decrease the oxidation rate of the interconnect [4]. Furthermore it has previously been reported that cerium resides mostly in the outer (spinel-) oxide layer when it is used for exposure times longer than 168 h [12,13]. In this context, the effect of cerium on the electrical properties of these types of coatings is interesting. A lower ASR can be expected since the oxide growth rate is decreased by the presence of cerium [14]. Besides the effects of a change in oxide chemistry, as reported by Canovic et al., and the reduced growth rate mentioned above, a doping effect of the cerium itself on the spinel layer might also be suspected. Impedance spectroscopy has rarely been used to study

* Corresponding author. Tel.: +46317722828; fax: +46317722853.

E-mail address: Jan.grolig@chalmers.se (J.G. Grolig).

the contribution of individual oxide layers that grow on a steel substrate. Impedance spectroscopy is a versatile non-destructive material testing method that can be used to give information about different time dependent conduction mechanisms in materials. It can be also used to investigate dielectric and electric properties, as well as properties such as growth, continuity or the presence of oxide layers [15,16]. Song et al. used impedance spectroscopy to examine oxide layers grown on AISI 304 and revealed the presence of a spinel oxide and a chromium oxide, the electrical properties of which could be determined [16]. Velraj et al. have presented impedance data on cobalt-plated Crofer 22 APU, where they observed three individual oxide layers; chromia, chromium containing cobalt oxide and a cobalt chromium spinel oxide [15].

Since there is already extensive literature available on different substrate materials with cobalt manganese coatings, this study aimed at investigating the effect of cerium on the electric properties of the cobalt manganese spinel oxide scale. The addition of cerium is expected to slow down the growth of the chromia, and, therefore, a lower area specific resistance (ASR) can be anticipated. The effects of cerium on the activation energy of the electrical conduction and the electrical properties of the outer spinel layer were investigated using a combination of classic DC characterization methods at high temperatures with impedance spectroscopy at low temperatures.

2. Experimental

2.1. Sample Preparation

Pre-coated steel sheets of Sanergy HT with a thickness of 0.2 mm were received from Sandvik Materials Technology. The composition of the substrate material is given in Table 1. The samples were coated with an industrially available physical vapor deposition method and consisted of either 640 nm cobalt or a double layer coating of a 10 nm layer of cerium (inner layer) and 640 nm of cobalt. For the deposition of both coating layers, metallic targets were used. The steel sheets were cut into coupons of $15 \times 15 \text{ mm}^2$. After ultrasonic cleaning with acetone and ethanol, the samples were weighed using a XP6 scale (Mettler Toledo).

2.2. Exposure

The samples were exposed at 850°C in tubular furnaces in simulated cathode atmosphere (air, 3% water vapor, flow of $27 \text{ cm}^3/\text{s}$), more information can be found in [17]. The water content was adjusted with a coil condenser and was maintained at thermodynamic equilibrium [17]. The samples were exposed isothermally for different durations of up to 3270 h.

2.3. Area specific resistance measurement

The samples were prepared for ASR characterization as shown in Fig. 1: A pre-oxidized sample was masked with a shadow mask of $10 \times 10 \text{ mm}^2$ and sputtered with platinum using a Quorum 150 sputter coater (60 mA and 10 min duration) to ensure a defined electrode area with an approximate platinum thickness of about 100 nm. This procedure was repeated for both sides of each sample. The electrodes were repainted with platinum ink (Metalor 6082) using a fine brush. The samples were then dried for 1.5 h at 150°C

and fired at 850°C for 10 min to burn off the binder of the platinum ink. The prepared samples were put into a ProboStat[®] sample holder with a four-point setup which was placed into a tubular furnace. The DC resistance of the samples was measured on two test stands using either a Keithley 2440 Current Source in combination with a Keithley 2701 digital multimeter or just a Keithley 2400 in four-point mode. A current density of $100 \text{ mA}/\text{cm}^2$ was applied during the measurement, and the ASR was measured at 50°C intervals from 850°C down to 500°C to enable an activation energy calculation. The measured resistance values were divided by two in order to obtain the ASR value for a single oxide scale. The measurements were performed using an ex-situ method, since it was previously shown that in-situ measurements affect the oxidation mechanism [18].

2.4. Impedance spectroscopy

For the impedance spectroscopy measurements, the same ProboStat[®] sample holder was used and placed into a tubular furnace. A Solartron 1260 Impedance Analyzer was used to measure in AC mode. A measurement potential of 100 mV without a bias was applied to measure the impedance of the samples in a frequency range from 10 mHz to 6 MHz. The impedance was measured at 10°C intervals in a temperature range from 200°C to 60°C . For the analysis and the fitting of the impedance data, ZView[®] software from Scribner was used.

3. Results

3.1. Gravimetric evolution

The mass gain of individual samples is plotted in Fig. 2. After an initial mass gain of $0.21 \text{ mg}/\text{cm}^2$ after only 2 h of exposure, the mass gain followed an almost parabolic trend. The cerium/cobalt coated samples showed a significantly lower mass gain than the cobalt coated samples. With exposure times longer than 1000 h, the mass gain of the cerium/cobalt coated samples was almost half as much as the cobalt coated samples. After 3300 h of exposure, an average mass gain of about $1.7 \text{ mg}/\text{cm}^2$ was observed for the cerium/cobalt coated samples in contrast to $2.8 \text{ mg}/\text{cm}^2$ for the cobalt coated samples.

3.2. DC characterization

The ASR of both cobalt and cerium/cobalt coated samples was measured at different time intervals from 2–3270 h. The evolution of the ASR values over time is plotted in Fig. 3. It can be seen that, over the entire exposure time, the ASR values of both sample systems increase. The cobalt coated samples were always significantly higher in ASR than the cerium/cobalt coated, even after the shortest exposure time of 2 h. The observed trend in ASR evolution was comparable to the previously shown mass gain. This can be also seen in Fig. 4, in which the relation between the mass gain and ASR is plotted, indicating an approximately linear relationship. However, some samples, especially the cobalt coated ones, showed a relative large spread. The activation energy of each measured sample was calculated using the Arrhenius equation. At very low mass gains and short exposure times, the activation energy was, for both sample systems, in the range of 0.55 to

Table 1
Sanergy HT composition in wt.% given by the supplier.

Fe	C	Si	Mn	P	S	Cr	Ni	Mo	W	Cu	Nb	Ti	N	Zr
Bal.	0.01	0.07	0.25	0.013	0.0005	22.39	0.81	0.93	<0.01	0.017	0.41	0.06	0.024	0.06

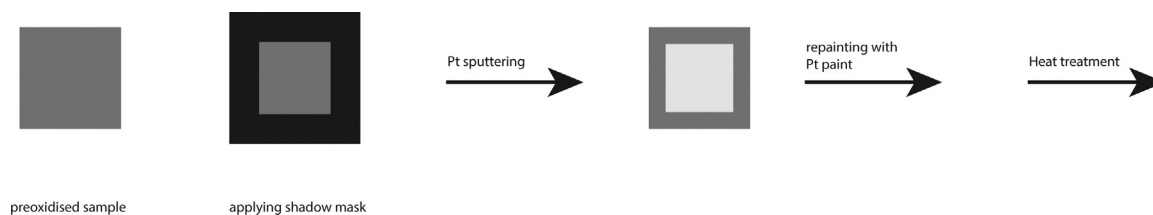


Fig. 1. Scheme of electrode preparation.

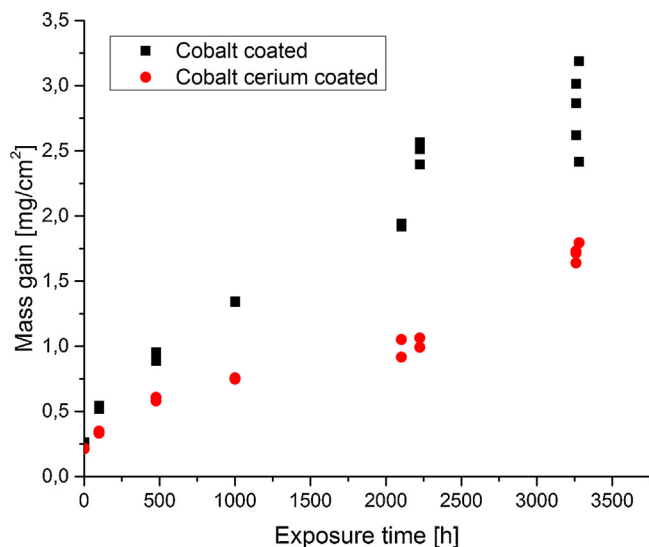


Fig. 2. Mass gain of individual samples over time.

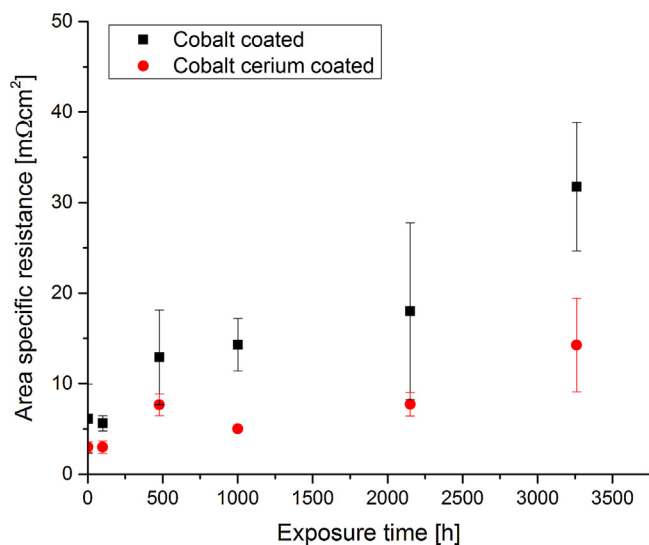


Fig. 3. Evolution of ASR values over time.

0.65 eV. Whereas at longer exposure times and high mass gain, the activation energy decreased to a value of about 0.45 eV, as can be seen in Fig. 5. No significant difference in activation energy was noted between cobalt coated and cerium/cobalt coated samples.

3.3. Impedance spectroscopy

Besides DC characterization, selected samples were also measured at lower temperatures using impedance spectroscopy. A representative Nyquist plot of a cobalt coated and a cerium/

cobalt coated sample exposed for 3300 h at 850 °C and measured at 150 °C is depicted in Fig. 6. For the temperature interval between 200 and 60 °C, two semi-circles for both samples could be recorded. An equivalent circuit of two R/CPE elements (R1/CPE1 and R2/CPE2) in series with an additional resistor (R3) was used for fitting (see inset Fig. 6). The additional resistor R3 which was in all cases significantly smaller than R1 and R2 represented the resistance of the bulk steel and the electrodes. The resulting resistances R1 and R2 of each temperature were used to calculate area specific conductivities, which were consequently plotted against the inverse temperature seen in Fig. 7. The conductivity for the cobalt coated sample was, for both R/CPE elements, much lower than the cerium/cobalt coated sample. Both samples showed similar activation energies for conductivity derived from the high frequency semi-circle with 0.40 eV for the cobalt coated sample and 0.45 eV for the cerium/cobalt coated sample. The activation energy for the conductivity derived from the low frequency semi-circle was 0.51 eV for the cobalt coated and 0.53 eV for the cerium/cobalt coated sample. Similar activation energies were observed for samples exposed for shorter exposure times. A compilation of resistance values, capacitance values and peak frequencies is shown in Tables 2 and 3.

3.4. Microstructural evolution

Over the entire exposure time, the microstructural evolution of both sample systems was in line with previously reported observations of similar coating and substrate combinations [9,10,13]. Cross-sections of a cobalt coated sample and a cerium/cobalt coated sample after 100 h of exposure and the electrical characterization of the samples are shown in Fig. 8a and b. Whereas in Fig. 9a and b, two cross-sections of a cobalt coated sample and a cerium/cobalt coated sample after more than 3000 h of exposure, including electrical characterization are shown. After 100 h of exposure, a double layered oxide was observed on both samples with a relatively thick outer oxide and a relatively thin inner oxide. Previously reported EDX analyses revealed that the outer oxide layer contained oxygen, cobalt, manganese and iron in the cobalt coated case, and oxygen, cobalt and manganese in the cerium/cobalt coated case [9]. The very thin inner oxide mainly consisted of chromium oxide [9]. After 3300 h (Fig. 9), a much thicker oxide scale was observed. The outer oxide scale, in both cases did not grow significantly. However, on the cobalt coated sample, a much thicker inner oxide with a thickness of approximately 10 μm, compared to a 5 μm thick inner oxide in the cerium/cobalt coated case, was observed, examining SEM cross-sections of several samples at different locations.

4. Discussion

4.1. Corrosion mechanism

The corrosion mechanism of these types of coatings has been extensively studied in previous publications [4,9–11,13,19]. Generally, the mechanism can be summarized as follows: The cobalt

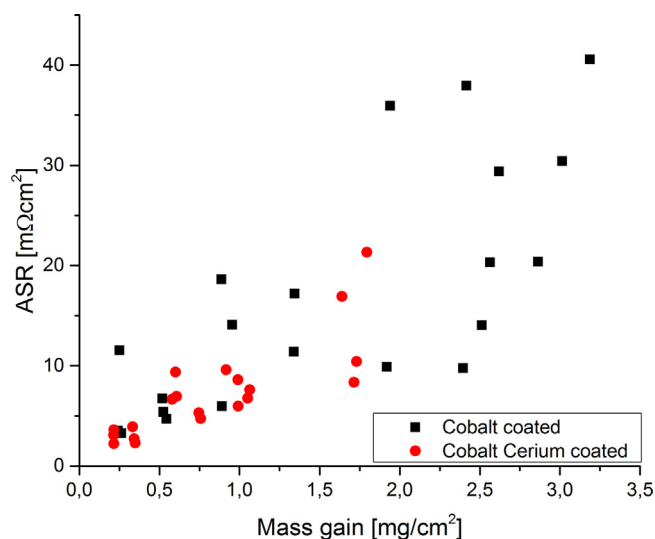


Fig. 4. Mass gain of individual samples plotted against ASR values.

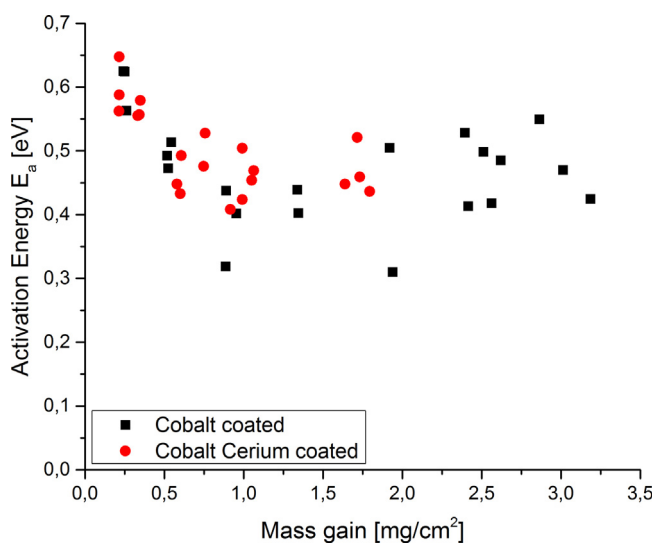


Fig. 5. Activation energy of individual samples over mass gain.

coating oxidizes in the very first moments of exposure to Co_3O_4 . When no cerium is present, a substantial amount of iron diffuses into the cobalt coating during the first heating. In the first 200 h of exposure, manganese, present in the steel, diffuses outwards and together with the cobalt oxide forms a cobalt manganese spinel, in the form of $(\text{Co,Mn,Fe})_3\text{O}_4$, with a stoichiometry ranging from $\text{Co}_{1.4}\text{Fe}_1\text{Mn}_{0.6}\text{O}_4$ at the innermost part of the oxide to $\text{Co}_{2.3}\text{Fe}_{0.4}\text{Mn}_{0.3}\text{O}_4$ at the oxide surface [9]. The ratio between cobalt and manganese depends on the amount of manganese present in the steel, the duration of exposure and the thickness of the cobalt coating. In the present case, the ratio of cobalt to manganese was about 2:1 for both used coatings after exposure times longer than 200 h. Over the entire exposure time, an oxide layer of chromia grew underneath the spinel oxide. When a double layer of cerium and cobalt was used as the coating, the diffusion of iron is inhibited resulting in an outer spinel oxide in the form of $(\text{Co,Mn})_3\text{O}_4$ and a drastically reduced chromia growth was observed. After an exposure time of 3300 h, an average chromia thickness of approximately 10 μm and 5 μm for the cobalt and cerium/cobalt coatings respectively had been obtained.

4.2. ASR evolution

The ASR values of the samples were expected to be mainly dominated by the growing oxide scales. Since the oxide scale after very short exposure times is mainly comprised of the outer cobalt manganese spinel, it can be assumed that the corresponding ASR value and especially activation energy will be largely determined by the electric properties of this spinel layer. The activation energy for the electrical conduction was determined to be 0.6 eV after only 2 h of exposure. Literature values available for the activation energy of cobalt manganese spinels are in the range of 0.76–0.55 eV [20–23]. By increasing exposure time, the inner oxide scale (Cr_2O_3) increased in thickness, whereas the outer spinel grows only minimally after about a week of exposure (168 h) [10]. Since the conductivity of chromia is several orders of magnitude lower than the conductivity of the cobalt manganese spinel, it was expected that the ASR values would be dominated by the inner chromia layer as soon as it had grown to sufficient thickness [21]. Additionally, the activation energy decreased to a value of about 0.45 eV over the investigated time frame, which might be seen as an indication of a change from a cobalt manganese spinel dominated conduction for exposure times shorter than 100 h to a chromia dominated conduction. Literature values for the activation energy of low temperature electronic conduction of chromia range from 0.18 eV up to 0.6 eV [24–28]. It has been mentioned by other researchers that this large spread might be due to the long equilibrium times and the high sensitivity of chromia conductivity to impurities [24–26,28,29]. An obvious observation in comparing the samples exposed for short times was the higher ASR of the cobalt coated samples than the cerium/cobalt coated samples. After only two hours of exposure, not a large difference in effective thickness of the chromia layer can be expected. If it is assumed that the outer spinel oxide layer of the sample dominates its conductivity after these short exposure times, the chemical difference in the outer spinel layer must cause the difference in ASR values for the two sample systems. A reason for this could be the higher amount of iron observed in the outer spinel layer. Kiefer et al. have reported a decrease in conductivity for $\text{MnCo}_{(2-x)}\text{Fe}_x\text{O}_4$ when x was more than 0.25, but reported an increasing conductivity when x was 0.1–0.25 [30]. Liu et al. observed a similar effect when investigating a spinel of the same composition, in contrast to the previous publication, only decreasing conductivity was observed when iron was added [23]. In a previous study on the same materials, an iron to manganese ratio of about 1:1 was seen for the cobalt coated samples [9]. Based on the two previous mentioned papers, this would lead only to a decrease of the conductivity of the cobalt manganese spinel. Cerium/cobalt coated samples contained only very small amounts of iron (below the quantitative EDX detection limit). For this reason, it is possible that the outward diffusion of iron caused the difference in conductivity. Another possibility could be an effect of cerium doping, which could have the potential to improve the conductivity of the spinel oxide layer of the cerium/cobalt coated samples, even though there is no literature available to support that theory.

If the ASR values after longer exposure times are mainly dominated by the growing chromia layer, as suspected above and, which can be also seen in the plot of the evolution of the activation energy (Fig. 5), the beneficial effect of a better conducting outer spinel becomes negligible. Therefore, the technique of impedance spectroscopy was used to investigate the influence of both oxide layers after longer exposure times. Since this technique works best at high resistance and capacitances, temperatures below 200 °C were chosen for the characterization. The two semicircles shown in Fig. 6 could be observed for both tested samples in a temperature range from 200–60 °C, which resulted in two slopes for each sample in the derived Arrhenius plot. The difficulty with

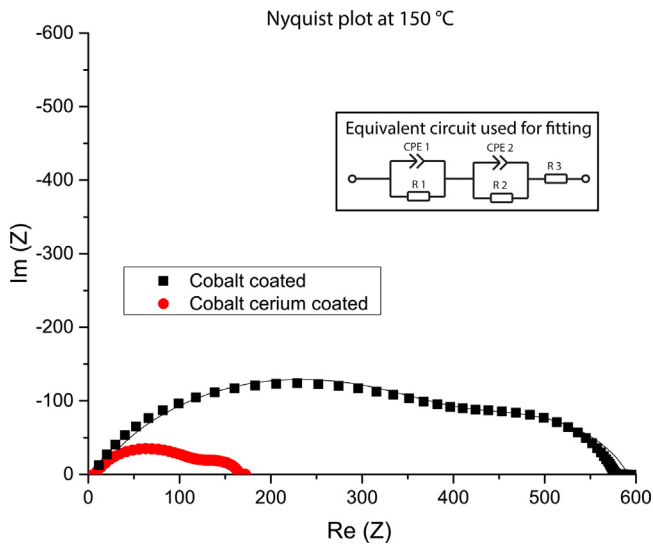


Fig. 6. Nyquist plot 150 °C of two samples exposed for 3300 h.

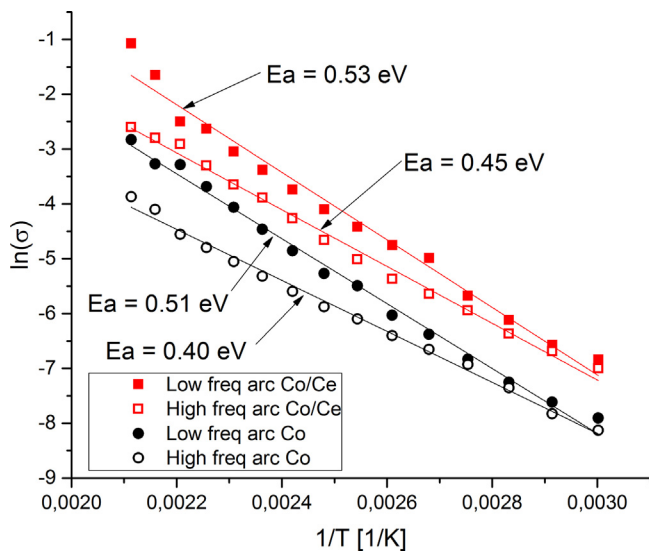


Fig. 7. Arrhenius plot of two samples exposed for 3300h derived from fitted Nyquist plots including activation energies.

impedance spectroscopy is assigning the individual semi-circles to the individual oxide scales. In the investigated case, two ways seemed to be appropriate to resolve this problem. The activation energies and/or the peak frequencies could be used to link the conductivities to the two oxide layers. Since the peak frequency of an RC element (or in this case R/CPE element) is proportional to the inverse of the product of capacitance and resistance and as the cobalt manganese spinel layer is much thinner and thus has likely a higher capacitance, but both oxide layers have similar resistances at these low temperatures, it can be assumed that the low frequency arc was caused by the cobalt manganese spinel layer. Another argument for this conclusion is the higher activation energy observed for the low frequency arc. The samples with very short exposure times had an activation energy of 0.6–0.55 eV, and, as discussed earlier, this was caused by the cobalt manganese spinel oxide layer. The low frequency arc in both cases (cobalt coated and cerium/cobalt coated) also had an activation energy in the range of 0.50–0.55 eV, and, based on this argument, would represent the cobalt manganese spinel layer. The higher amount of iron in the outer spinel of the cobalt coated sample is not expected to drastically change the activation energy, which is in agreement to Liu et al. [23]. Thus both ways of assigning the semi-circles to the individual oxide scales result in the fact that the low frequency arc is caused by the cobalt manganese spinel layer. However, it cannot be excluded that other effects, such as grain boundary and grain conductivity of for example the chromia layer influenced the measurement. Remarkable for the plot in Fig. 6 is the higher resistivity of the cobalt coated sample, observed for the low frequency arc, when compared to the cerium/cobalt coated sample. This supports the observation that after very short exposure times the resistance of the spinel layer for the cobalt coated samples was found to be higher. This would mean that the conductivity of the spinel layer is improved over the entire exposure time by the addition of cerium.

Since this investigation was performed at a temperature of 850 °C, the beneficial effect of cerium on the conductivity of the outer spinel layer becomes rather small. The actual operation temperature of a solid oxide fuel cell is often lower (600–800 °C) which might lead to a higher impact onto the overall ASR when the same materials would be used at lower temperatures. The chromia layer at lower temperatures grows significantly less at the same length of exposure and is considered to have a lower activation energy, thus, a higher impact of the outer spinel layer on the ASR can be expected [31]. Additionally, the use of a thicker cobalt manganese layer might be considered, since the investigated coating thickness was 640 nm, which is rather thin compared to the coatings reported in similar publications [32].

Table 2
Impedance data for cobalt coated sample.

Temperature [°C]	R1 [Ωcm ²]	C1 [F]	ω _{peak 1} [Hz]	R2 [Ωcm ²]	C2 [F]	ω _{peak 2} [Hz]	R3 [Ω]
200	96	1,9E-09	5,5E+06	34	2,1E-07	1,4E+05	10
190	121	1,7E-09	4,9E+06	53	1,6E-07	1,2E+05	10
180	190	1,4E-09	3,8E+06	53	2,7E-07	7,0E+04	10
170	242	1,9E-09	2,2E+06	80	3,7E-07	3,4E+04	10
160	313	1,8E-09	1,8E+06	116	2,9E-07	3,0E+04	10
150	408	1,7E-09	1,5E+06	174	2,3E-07	2,5E+04	10
140	537	1,6E-09	1,2E+06	257	1,9E-07	2,0E+04	10
130	712	1,6E-09	8,9E+05	390	1,6E-07	1,6E+04	10
120	889	1,6E-09	7,2E+05	486	1,5E-07	1,3E+04	10
110	1206	1,5E-09	5,5E+05	833	1,1E-07	1,1E+04	10
100	1555	1,5E-09	4,3E+05	1175	9,6E-08	8,9E+03	10
90	2047	1,5E-09	3,3E+05	1859	7,4E-08	7,3E+03	10
80	3123	1,6E-09	2,0E+05	2823	8,2E-08	4,3E+03	10
70	5016	1,7E-09	1,2E+05	4062	1,1E-07	2,3E+03	10
60	6791	1,7E-09	8,7E+04	5421	1,0E-07	1,8E+03	10

Table 3
Impedance data for cerium/cobalt coated sample..

Temperature [°C]	R1 [Ωcm^2]	C1 [F]	$\omega_{\text{peak 1}}$ [Hz]	R2 [Ωcm^2]	C2 [F]	$\omega_{\text{peak 2}}$ [Hz]	R3 [Ω]
200	27	9,7E-09	3,9E+06	6	2,8E-06	6,1E+04	10
190	33	6,8E-09	4,5E+06	10	1,6E-06	6,1E+04	10
180	37	5,7E-09	4,8E+06	24	4,8E-07	8,5E+04	10
170	54	4,4E-09	4,2E+06	28	6,5E-07	5,6E+04	10
160	77	3,8E-09	3,4E+06	42	5,6E-07	4,3E+04	10
150	97	3,5E-09	2,9E+06	59	4,5E-07	3,8E+04	10
140	142	3,3E-09	2,2E+06	84	4,7E-07	2,5E+04	10
130	212	3,2E-09	1,5E+06	120	5,1E-07	1,6E+04	10
120	300	3,1E-09	1,1E+06	166	5,5E-07	1,1E+04	10
110	430	3,2E-09	7,3E+05	232	5,8E-07	7,4E+03	10
100	562	3,2E-09	5,5E+05	293	6,1E-07	5,6E+03	10
90	761	3,0E-09	4,4E+05	582	3,2E-07	5,4E+03	10
80	1163	3,0E-09	2,9E+05	903	3,1E-07	3,5E+03	10
70	1607	3,0E-09	2,1E+05	1427	2,7E-07	2,6E+03	10
60	2189	3,0E-09	1,5E+05	1869	2,4E-07	2,2E+03	10

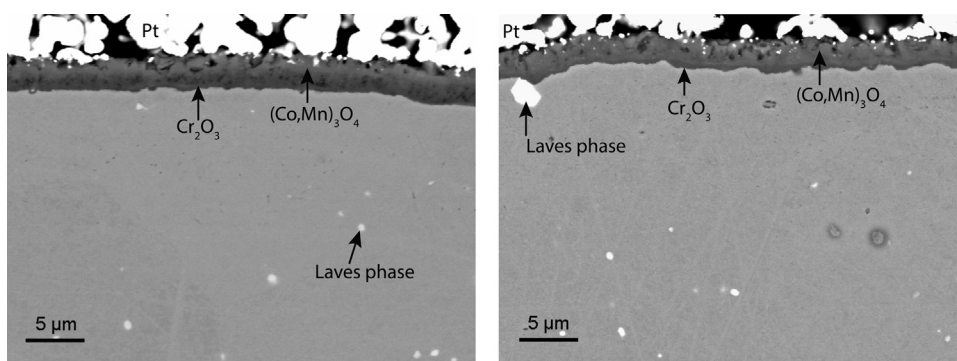


Fig. 8. SEM cross-sections of a cobalt coated sample (left) and cobalt cerium coated sample after 100 h of exposure and ASR characterization.

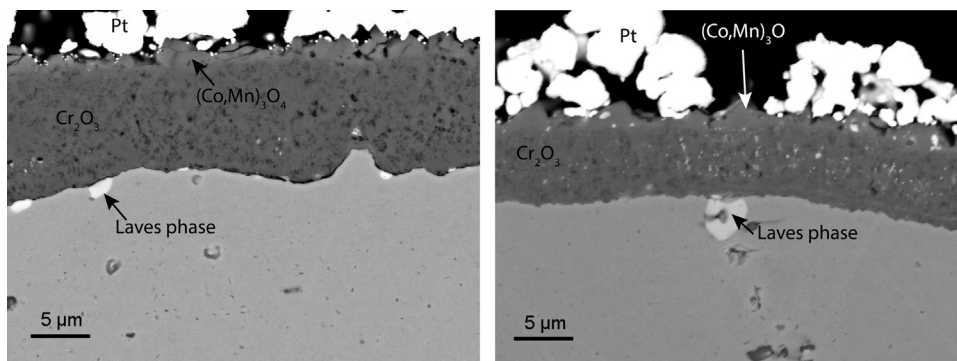


Fig. 9. SEM cross-sections of a cobalt coated sample (left) and cobalt cerium coated sample after more than 3000 h of exposure and ASR characterization.

5. Conclusion

The electrical performance of 640 nm cobalt and 640 nm cobalt in combination with 10 nm cerium on the stainless steel Sanergy HT in an air environment at 850 °C was investigated. It was observed that cerium improved the corrosion properties of Sanergy HT substantially by slowing down the growth of chromia. Due to the thinner chromia layer, the electrical properties of the samples were significantly better than those samples, which were only cobalt coated. Moreover, the addition of cerium prevented the outward diffusion of iron, which proved to be beneficial for the conductivity of the outer spinel oxide. Impedance spectroscopy was successfully used to reveal individual electrical properties of

the two oxide layers present after long exposure times. The ASR values of the investigated sample systems were dominated by the cobalt manganese spinel layer for short exposure times (less than 100 h) and, after longer times, by the growing and less conductive chromia layer. It was found that the cobalt manganese spinel layer had an activation energy for the electrical conduction of about 0.55 eV, whereas the inner chromia layer exhibited an activation energy of about 0.45 eV. At the investigated temperature of 850 °C, the effect of a better conducting spinel layer onto the overall conductivity was rather small for long exposure times. Yet, a much higher positive impact was expected, when these kinds of coatings are used at lower temperature, where a thinner chromia scale is expected.

Acknowledgements

P. Alnegren, H. Falk-Windisch and R. Sachitanand are gratefully acknowledged for proof-reading and valuable input during the discussion of the paper. Sandvik Materials Technology is acknowledged for providing the samples. The financial support received from The Swedish Research Council and Swedish Energy Agency (Grant Agreement No 34140-1), The Swedish High Temperature Corrosion Centre as well as the Nordic NaCoSOFC project is gratefully acknowledged. Furthermore, the funding received from the European Union's Seventh Framework Programme (FP7/2007-2013) for the Fuel Cells and Hydrogen Joint Technology Initiative under grant agreement n°[278257] is thankfully acknowledged.

References

- [1] R. Sachitanand, M. Sattari, J.-E. Svensson, J. Froitzheim, Evaluation of the oxidation and Cr evaporation properties of selected FeCr alloys used as SOFC interconnects, *Int. J. Hydrog. Energy* 38 (2013) 15328–15334.
- [2] D.E. Alman, P.D. Jablonski, Effect of minor elements and a Ce surface treatment on the oxidation behavior of an Fe-22Cr-0.5Mn (Crofer 22 APU) ferritic stainless steel, *Int. J. Hydrog. Energy* 32 (2007) 3743–3753.
- [3] M. Stanislawski, E. Wessel, K. Hilpert, T. Markus, L. Singheiser, Chromium vaporization from high-temperature alloys I. Chromia-forming steels and the influence of outer oxide layers, *J. Electrochem. Soc.* 154 (2007) A295–A306.
- [4] J.G. Grolig, J. Froitzheim, J.E. Svensson, Coated stainless steel 441 as interconnect material for solid oxide fuel cells: Oxidation performance and chromium evaporation, *J. Power Sources* 248 (2014) 1007–1013.
- [5] P.D. Jablonski, C.J. Cowen, J.S. Sears, Exploration of alloy 441 chemistry for solid oxide fuel cell interconnect application, *J. Power Sources* 195 (2010) 813–820.
- [6] I. Belogolovsky, P.Y. Hou, C.P. Jacobson, S.J. Visco, Chromia scale adhesion on 430 stainless steel: Effect of different surface treatments, *J. Power Sources* 182 (2008) 259–264.
- [7] M. Linder, T. Hocker, L. Holzer, K.A. Friedrich, B. Iwanschitz, A. Mai, J.A. Schuler, Cr₂O₃ scale growth rates on metallic interconnectors derived from 40,000 h solid oxide fuel cell stack operation, *J. Power Sources* 243 (2013) 508–518.
- [8] J.G. Grolig, H. Abdesselam, M. Gas, H.F. Windisch, J. Froitzheim, J.E. Svensson, Copper Based Conversion Coatings on Ferritic Stainless Strip Steel as Solid Oxide Fuel Cell Interconnects: Oxidation Performance and Chromium Evaporation, *Solid Oxide Fuel Cells 13 (Sofc-Xiii)* 57 (2013) 2339–2347.
- [9] S. Canovic, J. Froitzheim, R. Sachitanand, M. Nikumaa, M. Halvarsson, L.G. Johansson, J.E. Svensson, Oxidation of Co- and Ce-nanocoated FeCr steels: A microstructural investigation, *Surface and Coatings Technology* 215 (2013) 62–74.
- [10] J. Froitzheim, S. Canovic, M. Nikumaa, R. Sachitanand, L.G. Johansson, J.E. Svensson, Long term study of Cr evaporation and high temperature corrosion behaviour of Co coated ferritic steel for solid oxide fuel cell interconnects, *J. Power Sources* 220 (2012) 217–227.
- [11] J. Froitzheim, J.E. Svensson, Multifunctional Nano-Coatings for SOFC Interconnects, in: S.C. Singhal, K. Eguchi (Eds.), *Solid Oxide Fuel Cells*, vol. 12, Electrochemical Society Inc, Pennington, 2011, pp. 2503–2508.
- [12] M. Sattari, R. Sachitanand, J. Froitzheim, J.E. Svensson, T. Jonsson, The effect of Ce on the high temperature oxidation properties of a Fe–22%Cr steel: microstructural investigation and EELS analysis, *Mater. High Temp.* 32 (2015) 118–122.
- [13] R. Sachitanand (2011) unpublished work.
- [14] A. Magrasó, H. Falk-Windisch, J. Froitzheim, J.E. Svensson, R. Haugsrud, Reduced long term electrical resistance in Ce/Co-coated ferritic stainless steel for solid oxide fuel cell metallic interconnects, *Int. J. Hydrog. Energy* (2015) .
- [15] S. Velraj, J.H. Zhu, A.S. Painter, S.W. Du, Y.T. Li, Impedance spectroscopy of the oxide films formed during high temperature oxidation of a cobalt-plated ferritic alloy, *J. Power Sources* 247 (2014) 314–321.
- [16] S.H. Song, P. Xiao, An impedance spectroscopy study of oxide films formed during high temperature oxidation of an austenitic stainless steel, *J. Mater. Sci.* 38 (2003) 499–506.
- [17] J. Froitzheim, H. Ravash, E. Larsson, L.G. Johansson, J.E. Svensson, Investigation of Chromium Volatilization from FeCr Interconnects by a Denuder Technique, *J. Electrochem. Soc.* 157 (2010) B1295–B1300.
- [18] J.G. Grolig, J. Froitzheim, J.-E. Svensson, Coated stainless steel 441 as interconnect material for solid oxide fuel cells: Evolution of electrical properties, *J. Power Sources* 284 (2015) 321–327.
- [19] J. Froitzheim, A. Magraso, T. Holt, M.W. Lundberg, H.F. Windisch, R. Berger, R. Sachitanand, J. Westlinder, J.E. Svensson, R. Haugsrud, Nano Coated Interconnects for SOFC (NaCoSOFC), *Solid Oxide Fuel Cells 13 (Sofc-Xiii)* 57 (2013) 2187–2193.
- [20] X. Chen, P.Y. Hou, C.P. Jacobson, S.J. Visco, L.C. De Jonghe, Protective coating on stainless steel interconnect for SOFCs: oxidation kinetics and electrical properties, *Solid State Ion* 176 (2005) 425–433.
- [21] A. Petric, H. Ling, Electrical conductivity and thermal expansion of spinels at elevated temperatures, *J. Am. Ceram. Soc.* 90 (2007) 1515–1520.
- [22] Y.J. Liu, J.W. Fergus, C. Dela Cruz, Electrical Properties, Cation Distributions, and Thermal Expansion of Manganese Cobalt Chromite Spinel Oxides, *J. Am. Ceram. Soc.* 96 (2013) 1841–1846.
- [23] Y.J. Liu, J.W. Fergus, K.L. Wang, Dela Cruz C, Crystal Structure, Chemical Stabilities and Electrical Conductivity of Fe-Doped Manganese Cobalt Spinel Oxides for SOFC Interconnect Coatings, *J. Electrochem. Soc.* 160 (2013) F1316–F1321.
- [24] A. Holt, P. Kofstad, ELECTRICAL-CONDUCTIVITY AND DEFECT STRUCTURE OF CR2O3 .2. REDUCED TEMPERATURES (LESS-THAN-SIMILAR-TO-1000-DEGREES-C), *Solid State Ion.* 69 (1994) 137–143.
- [25] J.H. Park, K. Natesan, ELECTRONIC TRANSPORT IN THERMALLY GROWN CR2O3, *Oxid. Met.* 33 (1990) 31–54.
- [26] H. Nagai, T. Fujikawa, K. Shoji, ELECTRICAL-CONDUCTIVITY OF CR2O3 DOPED WITH LA2O3, Y2O3 AND NIO, *Transactions of the Japan Institute of Metals* 24 (1983) 581–588.
- [27] L.N. Cojocar (1969). ELECTRICAL PROPERTIES OF NON-STOICHIOMETRIC CR2O3, *Zeitschrift Fur Physikalische Chemie, Frankfurt*, 64 255–&.
- [28] D.B. Meadowcroft, F.G. Hicks, Electrical conduction processes and defect structure of chromic oxide, *Proc. Br. Ceram. Soc.* 23 (1972) 33–41.
- [29] A. Holt, P. Kofstad, ELECTRICAL-CONDUCTIVITY AND DEFECT STRUCTURE OF CR2O3 .1. HIGH-TEMPERATURES (GREATER-THAN-SIMILAR-TO-1000-DEGREES-C), *Solid State Ion.* 69 (1994) 127–136.
- [30] T. Kiefer, M. Zahid, F. Tietz, D. Stoeber, H.R. Zerrfass, Electrical conductivity and thermal expansion coefficients of spinels in the series MnCo_{2-x}FexO₄ for application as a protective layer in SOFC, *Risoe National Laboratory*, 2005, 2015 pp. 261–266.
- [31] H. Falk-Windisch, J.E. Svensson, J. Froitzheim, The effect of temperature on chromium vaporization and oxide scale growth on interconnect steels for Solid Oxide Fuel Cells, *J. Power Sources* 287 (2015) 25–35.
- [32] A. Harthoj, T. Holt, P. Moller, Oxidation behaviour and electrical properties of cobalt/ cerium oxide composite coatings for solid oxide fuel cell interconnects, *J. Power Sources* 281 (2015) 227–237.